Biogeotechnics 4 (2026) 100189

Contents lists available at ScienceDirect

Biogeotechnics

journal homepage: www.keaipublishing.com/en/journals/biogeotechnics/

Influence of end caps on the unconfined compressive strength of bio-cemented sand

Guijie Sang[a,*], Grainne El Mountassir[b], James M. Minto[b], Rebecca J. Lunn[b]

[a] Department of Civil and Environmental Engineering, University of Liverpool, Liverpool, UK
[b] Department of Civil and Environmental Engineering, University of Strathclyde, Glasgow, UK

ARTICLE INFO

Keywords:
Biocementation
Capping methods
Surface flatness
Density variation
UCS-$CaCO_3$ Relationship

ABSTRACT

Microbially induced carbonate precipitation (MICP) has been widely studied for enhancing soil strength, particularly through unconfined compressive strength (UCS) testing of treated sands. Many studies report correlations between UCS and calcium carbonate ($CaCO_3$) content, significant variability exists, often attributed to reagent properties, soil characteristics, injection strategies, and environmental conditions. However, the role of experimental testing procedures—especially end preparation and capping methods—has been largely overlooked. When preparing cylindrical specimens for UCS testing, conventional grinding methods often fail to achieve the required surface flatness, owing to the relatively weak bio-cementation bond. This shortcoming necessitates the use of appropriate capping methods to minimise stress concentrations induced by surface irregularities. In this study, we examined the effects of using two different end capping methods on the UCS of bio-cemented sand specimens: (1) bonded gypsum plaster caps (ASTM C617/C617M-15), and (2) unbonded silicone (rubber) caps (ASTM C1231/C1231M-15). The two end caps produced significantly different mechanical responses. Unbonded silicone-capped specimens exhibited more ductile behaviour, lower peak strengths, and stress-strain curves with multiple peaks and troughs—attributed to near-surface damage as the cap deforms. In contrast, bonded gypsum-capped specimens exhibited higher peak strengths at lower axial strains and smoother stress–strain curves. These behaviours are attributed to the much higher stiffness of cured gypsum plaster relative to the bio-cemented sand. Consequently, failure in these bonded specimens typically occurred at the weakest point (i.e. the least dense section as evidenced by X-ray radiography), with some showing well-defined shear bands across the sample length. The study also demonstrated that the measured UCS of bio-cemented sand is highly sensitive to density variations along the sample length, in addition to $CaCO_3$ content. To minimise the influence of surface irregularities on UCS results, it is therefore recommended that core specimens be capped with gypsum plaster in accordance with ASTM C617/C617M-15. The capping method should also be reported when presenting UCS data as it can significantly influence the mechanical response.

1. Introduction

Over the past two decades, extensive research has demonstrated the effectiveness of microbially induced carbonate precipitation (MICP) in enhancing soil strength, particularly through unconfined compressive strength (UCS) testing of MICP-treated sands (Al Qabany & Soga, 2013; Cheng et al., 2013, 2014, 2017; Choi et al., 2016; Cui et al., 2017; Gowthaman et al., 2019; D. Li et al., 2018; M. Li et al., 2017; Liu et al., 2019; Ma et al., 2022; Mahawish et al., 2016; Rowshanbakht et al., 2016; Sang et al., 2023, 2024a; Terzis & Laloui, 2018; van Paassen et al., 2010; Wu et al., 2020; P. Xiao et al., 2018; Y. Xiao et al., 2019). The majority of these studies have reported correlations between the calcium carbonate content within treated samples and their corresponding UCS values. However, significant variability exists among these reported relationships, as shown in Fig. 1A, often attributed to factors such as reagent characteristics (e.g. bacterial density, urease activity, chemical concentrations, pH), soil properties (e.g. gradation, density, particle shape and roughness, degree of saturation, fines content, mineralogy), injection strategies (e.g. fluid velocity, static periods, single or cyclic injection), and environmental conditions (e.g. temperature, pressure, oxic/anoxic environments, pore fluid salinity) (El Mountassir et al., 2018). These factors directly influence the total

* Corresponding author.
E-mail address: g.sang@liverpool.ac.uk (G. Sang).

https://doi.org/10.1016/j.bgtech.2025.100189
Received 12 May 2025; Received in revised form 8 June 2025; Accepted 17 June 2025
Available online 23 June 2025
2949-9291/© 2026 The Authors. Publishing services by Elsevier B.V. on behalf of KeAi Communications Co. Ltd. This is an open access article under the CC BY license (http://creativecommons.org/licenses/by/4.0/).

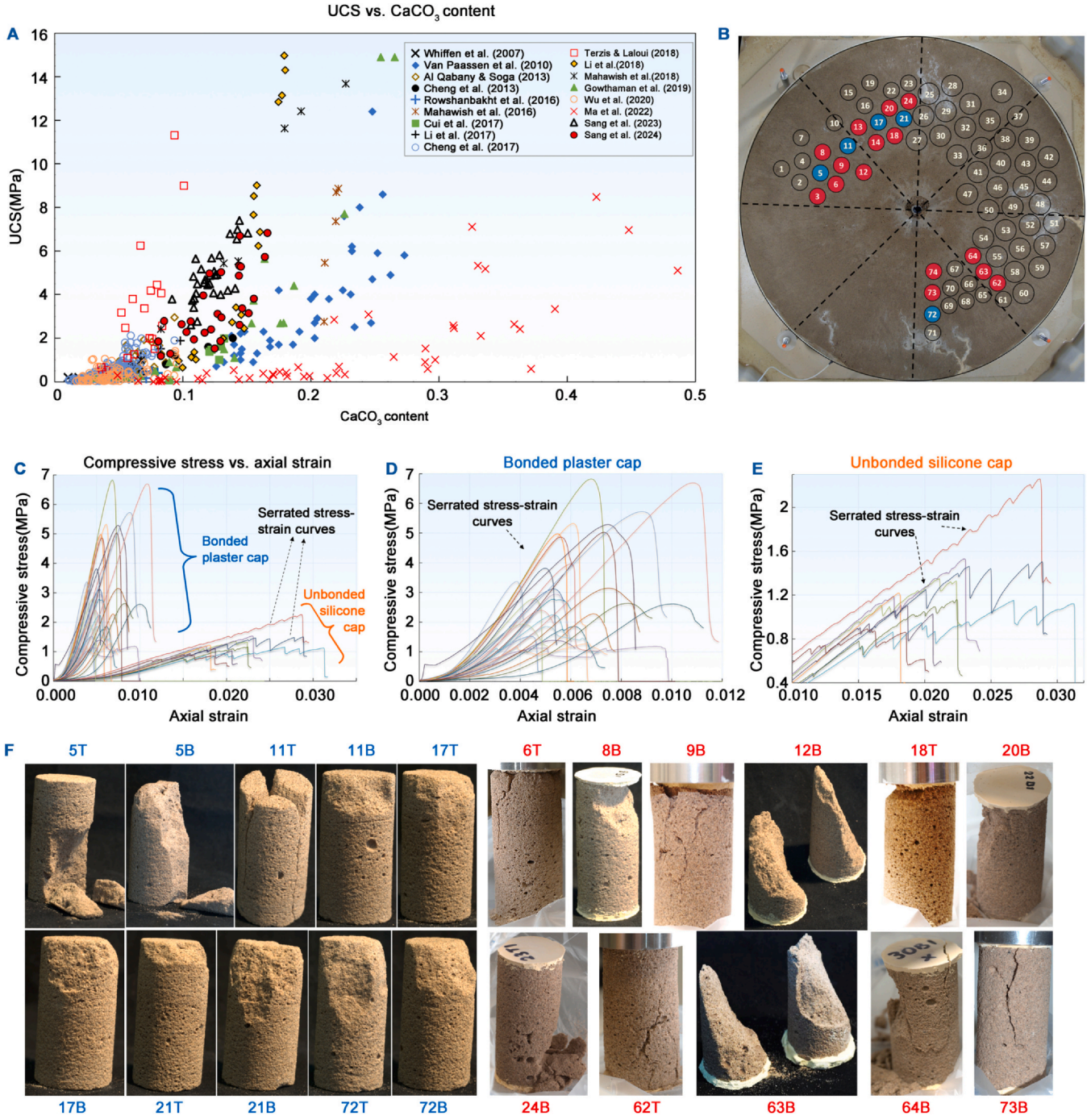


Fig. 1. (**A**) Variations in the UCS-$CaCO_3$ relationship of bio-cemented sand (Al Qabany & Soga, 2013; Cheng et al., 2013, 2017; Cui et al., 2017; Gowthaman et al., 2019; D. Li et al., 2018; M. Li et al., 2017; Ma et al., 2022; Mahawish et al., 2016, 2018; Rowshanbakht et al., 2016; Sang et al., 2023, 2024a; Terzis & Laloui, 2018; van Paassen et al., 2010; Whiffin et al., 2007; Wu et al., 2020), factors influencing the UCS-$CaCO_3$ relationship are summarised in a book chapter (El Mountassir et al., 2018); (**B**) Coring locations labelled with numbers in the radial flow cell (RFC). Ten samples capped with silicone pads (unbonded) were cut from five full-length cores (#5, #11, #17, #21, and #72), marked with blue circles, while the samples capped with gypsum plaster (bonded) were cut from full-length cores marked with red circles; (**C**) Compressive stress versus axial strain for all tested cores during UCS tests. Ten cores were capped with silicone pads (unbonded), whilst the remaining cores were capped with gypsum plaster (bonded); (**D–E**) Close-up views of the stress-strain curves for the unbonded and bonded cores, respectively; (**F**) Post-failure images of all unbonded samples (blue labels) and selected bonded samples (red labels). In the sample labels, the number indicates the drilling location (refer to Fig. S1, whilst the letters T and B denote half-length samples cut from the top and bottom sections of the full-length (150 mm) cores, respectively.

precipitation amount of calcium carbonate, its spatial distribution (i.e. uniformity), and effectiveness (e.g. inter-particle bridging, pore filling, surface coating), thereby causing significant variation of the UCS-$CaCO_3$ relationship.

However, experimental testing procedures can also influence significantly measured UCS values and may contribute to some of the observed variability in $CaCO_3$-UCS relationships reported in the literature. For instance, when preparing bio-cemented sand cores as cylindrical specimens for UCS testing, conventional end preparation methods—such as sanding with fine sandpaper or using grinding wheels designed for hard rock cores—often fail to achieve the required surface flatness, owing to the relatively weak bio-cementation bond

compared to cement bonded materials or rocks. Even minor surface defects can create local stress concentrations or inaccuracies in surface area measurement, both of which may lead to underestimated or unreliable UCS values. Therefore, appropriate capping methods are essential to minimise stress concentrations induced by surface irregularities, especially given that the measured strength of bio-cemented sand is already sensitive to various other factors, including $CaCO_3$ content and distribution, particle size, grain shape, among others.

In this study, we investigate the influence of two standard capping methods—bonded plaster capping in accordance with ASTM C617/C617M-15 and unbonded rubber capping following ASTM C1231/C1231M-15—on the UCS results of bio-cemented core samples. Two-dimensional (2D) X-ray radiography was employed to quantify internal density variations, and the $CaCO_3$ content near the failure plane was also measured. The results provide direct evidence that end conditions significantly affect UCS measurements and should therefore be carefully considered and consistently reported in UCS testing of bio-cemented materials.

2. Materials and methods

2.1. Core sampling

Full-length cylindrical cores (35 mm in diameter and 150 mm in length) were drilled from a radial flow cell (RFC) constructed in the laboratory, measuring approximately 1 m in diameter and 150 mm in thickness. The RFC was initially filled with poorly graded sand with a median grain size of 0.27 mm, a uniformity coefficient of 1.5, and a coefficient of curvature of 0.98. The sand was then treated using MICP. The RFC featured a central injection well designed to generate a radial flow pattern for the delivery of MICP treatment fluids. Effective treatment was achieved after nine MICP cycles using a two-phase injection strategy. Details of the MICP experiments are provided in a recent study (Sang et al., 2024b). The core sampling locations within the RFC are shown in Fig. 1B.

2.2. UCS test and $CaCO_3$ content

The full-length cores (150 mm) were cut in half to produce specimens with a length-to-diameter ratio of approximately 2:1. Each specimen was labelled with a number corresponding to the drilling location (refer to Fig. 1B), whilst the letters 'T' and 'B' indicate half-length samples taken from the top and bottom sections, respectively, of the full-length (150 mm) cores. The end surfaces of each cylindrical specimen were polished using sandpaper and then capped with either (1) gypsum plaster (Crystacast, compressive strength: 55.2 MPa, plaster-to-water ratio: 100/28), in accordance with ASTM C617/C617M-15, or (2) an unbonded silicone rubber pad, following ASTM C1231/C1231M-15. The former is classified as a bonded plaster cap, whilst the latter is considered an unbonded silicone cap. Both capping methods were applied to ensure smooth, flat ends and to minimise the effects of stress concentrations that can arise from uneven loading surfaces. Prior to the UCS tests, all core specimens were oven-dried at 60 °C until no further mass loss was observed. The UCS test was conducted in accordance with ASTM D4219-08, using a constant displacement rate of 0.2 mm/min. Each test was terminated after a clear peak strength was reached. Images of the post-failure specimens were subsequently collected.

After UCS testing, the $CaCO_3$ content of each core was determined using the acid washing method, based on ~30–60 g of sample collected near the failure plane. Further details on the determination of $CaCO_3$ content are provided in a previous study (Sang et al., 2024b).

2.3. 2D X-ray radiography

The bulk density of the UCS-tested cores was estimated using the dimensions of the cylindrical cores and their dry weight. However, due to slight irregularities in core diameter along their length and surface unevenness, this method may introduce bias in the estimation of bulk density for the bio-cemented cores. To improve the accuracy of bulk density estimation and assess density variations with depth, thirteen full-length core samples and one 10 cm-long core sample retrieved from the RFC were subjected to 2D X-ray radiography scans at both 0° and 90° orientations (refer to Supplementary Figure S1). The X-ray scanning was performed at 150 kV and 166 μA, with an exposure time of 708 ms and a voxel size of 90 μm. Single shading correction was applied to all scans, and each image represented the average of 16 frames to enhance image quality. The derivation of the density variation with depth for each core sample is provided in Supplementary Section S2.

3. Results and discussion

3.1. Effect of end caps on mechanical responses

The UCS curves based on the two capping methods are shown in Fig. 1C. Samples capped with bonded plaster showed smoother stress–strain responses, higher UCS values, and lower axial strains. In contrast, those capped with the unbonded silicone pad exhibited serrated stress–strain curves, lower UCS, and higher axial strains. It is worth noting that the bonded and unbonded core samples were drilled in close proximity (see Fig. 1B for their locations) and exhibit similar ranges of $CaCO_3$ content (0.08–0.19), bulk density (1500–1800 g/cm^3), and density variation along the depth, as detailed in the next section. The more ductile behaviour observed in the unbonded samples—evidenced by the greater axial strain at peak strength—can be attributed to deformation of the silicone pad used for unbonded end capping. This deformation, combined with the interfacial friction between the silicone pad and specimen end, likely resulted in stress concentrations near the sample ends, leading to localised damage (as evident in the post-failure images in Fig. 1F for most unbonded samples) and consequently serrated stress–strain behaviour during loading (Fig. 1E). These localised failures contributed to the overall reduction in peak strength observed in the unbonded samples (Fig. 1C). For example, among the ten unbonded samples, samples 11B, 17T, 17B, 21T, 21B, 72T, and 72B all failed at the top end near the silicone pad (Fig. 1F). Of these, samples 11B,17T, 17B, 21T, 21B exhibited lower density near the top end as shown in Fig. 2(B–D), whereas samples72T and 72B showed a relatively uniform density along their length as shown in Fig. 2E. Notably, samples 5T, 5B, and 11T failed in a tensile mode—at positions of lower density in samples 5T and 5B (Fig. 2A), and along the entire length in sample 11T (Fig. 2B). This splitting failure was most likely caused by lateral frictional forces at the sample ends, induced by the lateral expansion of the silicone pad during loading.

Compared to the unbonded silicone pad cap, the cured gypsum plaster cap at the sample ends was significantly stiffer and the interfacial friction between the loading steel platen and the gypsum-capped specimen surface was lower than that with the silicone pad; thus, the axial strain observed in the gypsum-bonded samples more accurately reflected the true deformation behaviour of the bio-cemented sand. These bonded samples failed at various positions along their depth (Fig. 1) without exhibiting serrated stress–strain responses during loading (Fig. 1D). The failure locations were mostly concentrated at points of lowest density (i.e. the weakest zones) along the length of each core, as observed in samples 6T, 9B, 18T, 24B, 62T, 64B (Fig. 2G–M). Moreover, samples 12B and 63B exhibited distinct shear bands along their length, characteristic of the brittle failure commonly observed in rock-like materials.

3.2. Effects of $CaCO_3$ content, bulk density, and density uniformity on UCS

Fig. 3A and B show the UCS values plotted against $CaCO_3$ content and bulk density (estimated from 2D X-ray radiography), respectively. A positive correlation between UCS and $CaCO_3$ content is observed for both bonded and unbonded samples, consistent with findings from

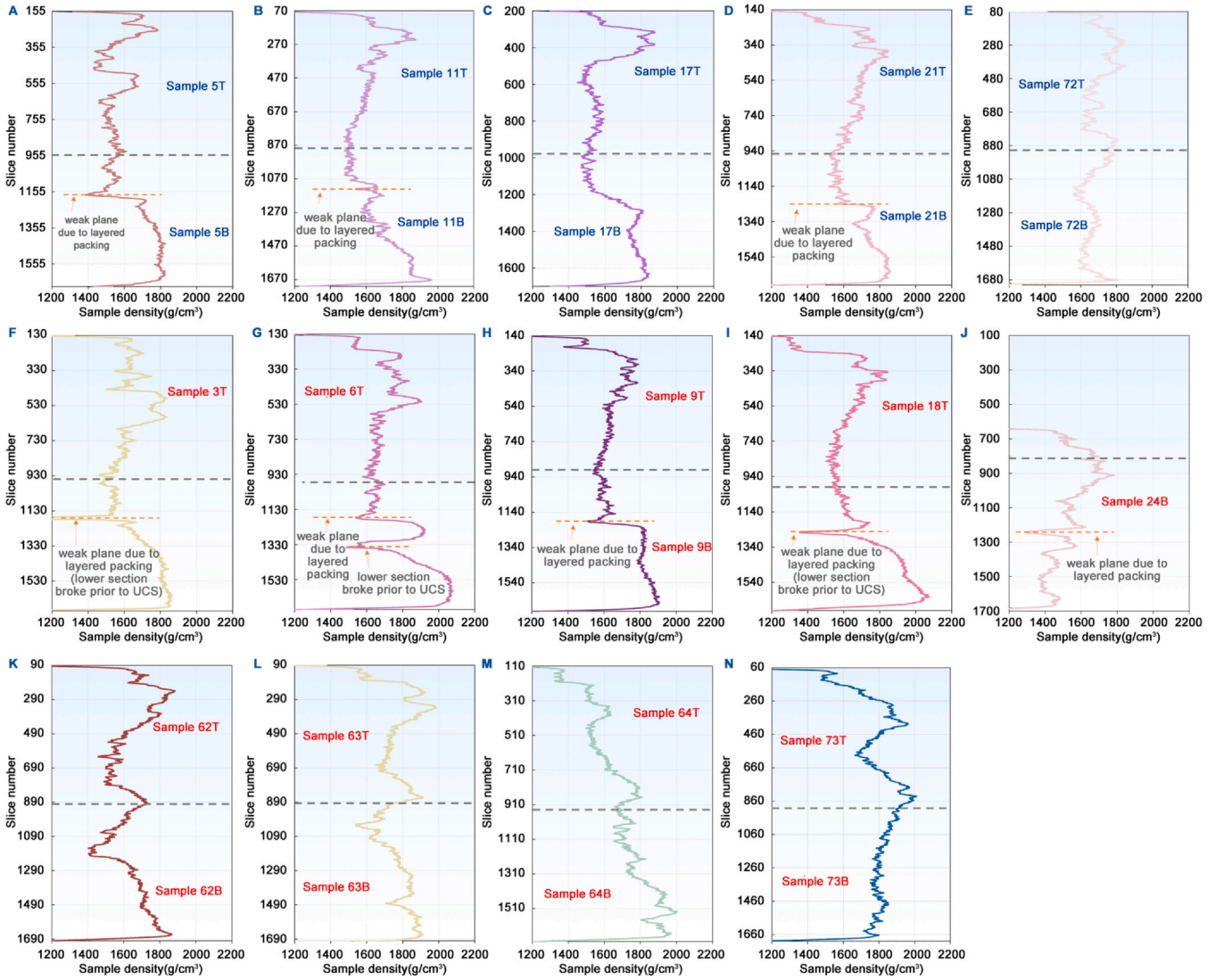


Fig. 2. Bulk density variation along slice number for thirteen full-length core samples and one 10 cm-long core sample (24B), averaged from 2D radiography scans taken at 0° and 90° orientations. The *y*-axis represents slice number, with a spacing of 0.09 mm between slices. (**A–E**) UCS-tested half-length samples capped with unbonded silicone pads are marked with blue labels; (**F–N**) Whilst those capped with bonded gypsum plaster are marked with red labels.

previous studies (Al Qabany & Soga, 2013; Cheng et al., 2017, 2014, 2013; Choi et al., 2016; Cui et al., 2017; Gowthaman et al., 2019; Li et al., 2018, 2017; Mahawish et al., 2016; Rowshanbakht et al., 2016; Sang et al., 2024b, 2023; Terzis & Laloui, 2018; van Paassen et al., 2010; Wu et al., 2020). However, despite having a similar range of $CaCO_3$ content (0.08–0.19), the unbonded samples exhibited significantly lower UCS values (0.9–2.3 MPa) compared to the bonded samples (1.2–6.8 MPa), likely due to localised damages near the sample end, as discussed previously. After UCS testing, six unbonded samples (11B-Re, 17T-Re, 17B-Re, 21T-Re, 21B-Re, and 72B-Re, post-failed samples are shown in Fig. 1F) were trimmed at the top end, recapped with gypsum plaster, and re-tested for UCS and $CaCO_3$ content (measured at the failure zones). The UCS–$CaCO_3$ plot for these re-tested samples (indicated by hollow black circles in Fig. 3A) aligns with the trend observed for the bonded samples.

A positive correlation between UCS and bulk density is observed for the bonded samples, whereas no clear correlation is found for the unbonded samples (Fig. 3B). The bulk density of each sample is determined by both the initial sand density (due to sand packing prior to MICP treatment) and the precipitated $CaCO_3$ content (after MICP treatment). In the bonded samples, the positive correlation between UCS and bulk density can be attributed due to (i) higher $CaCO_3$ content (ii) greater uniformity in density along the depth, or (iii) a combination of both factors. For example, samples 73B and 73 T, cut from the same full-length core (#73), exhibited similar bulk densities (Fig. 3B). However, sample 73B showed a higher $CaCO_3$ content (Fig. 3A) and greater density uniformity (Fig. 2N), which resulted in a higher UCS value compared to 73T. Similarly, sample 63B exhibited a higher UCS value than sample 63T, despite their comparable bulk density (Fig. 3B), due to its higher $CaCO_3$ content (Fig. 3A) and greater density uniformity (Fig. 2L). In contrast, the higher UCS values observed for samples 64B and 9B, compared to 64T and 9T, are primarily attributed to their higher $CaCO_3$ content (Fig. 3A) and higher bulk density (Fig. 3B), which partly results from a higher initial packing density (Fig. 2H), as evidenced in a previous study (Sang et al., 2024b).

Moreover, as shown in Fig. 3B, within bulk density ranges of 1550–1750 g/cm^3, the unbonded samples exhibited lower UCS values (0.9–2.3 MPa) compared to the bonded samples (1.4–4.0 MPa). The six re-bonded and re-tested samples (11B-Re, 17T-Re, 17B-Re, 21T-Re, 21B-Re, and 72B-Re, marked by hollow black circles in Fig. 3B) also exhibited positive UCS-density correlation, and exhibited even higher UCS values than the initially bonded samples. This is due to their shorter length, as the weakest sections near the sample ends were removed prior to UCS re-testing.

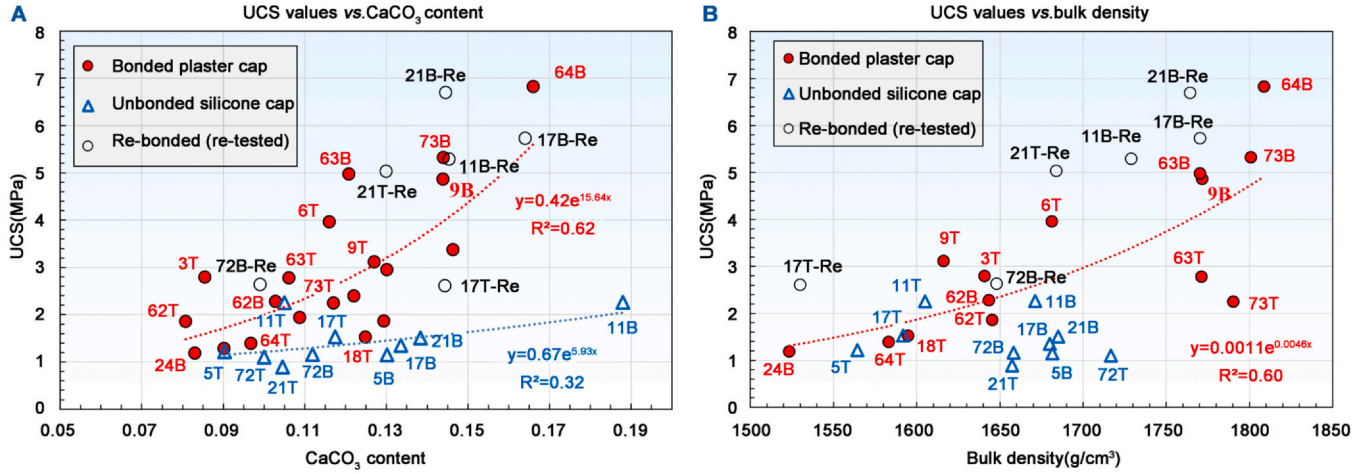


Fig. 3. (**A**) UCS values plotted against $CaCO_3$ content (measured at the failure plane). Red solid circles represent cores tested with bonded plaster caps (only 2D radiography scanned sampled were labelled), whilst blue triangles represent cores tested with unbonded silicone caps; (**B**) UCS values of the cores versus bulk density estimated based on 2D X-ray radiography. After UCS testing, six of the unbonded cores (11B, 17T, 17B, 21T, 21B, 72B) that failed near the top boundary were trimmed and recapped with plaster for retesting. Note: the length-to-diameter ratios of these six cores are less than 2, ranging from 1.2 to 1.7. The black hollow circles in represent the re-tested cores. The UCS–$CaCO_3$ and UCS–bulk density relationships were fitted using a power law, with fitting parameters listed in (A) and (B), respectively. No strong UCS–bulk density correlation was observed for the unbonded samples.

4. Conclusion

This study investigates the influence of two end caps—bonded gypsum plaster and unbonded silicone pads—on the UCS results of bio-cemented sand. We found that samples capped with gypsum plaster exhibited more consistent stress–strain curves and reliable UCS values, whereas those capped with silicone pads showed serrated stress–strain responses and more localised damage near the ends, leading to significant underestimation of UCS values. The study also highlights that the UCS of bio-cemented sand is highly sensitive to $CaCO_3$ content and density variations along the sample length. Therefore, it is essential to use and report appropriate capping methods (such as gypsum plaster) during UCS testing to minimise uncertainties and bias in the UCS–$CaCO_3$ relationship caused by end surface irregularities.

CRediT authorship contribution statement

Rebecca J. Lunn: Investigation, Writing – review & editing, Funding acquisition, Supervision. **James M. Minto:** Visualization, Formal analysis, Writing – review & editing, Data curation. **Grainne El Mountassir:** Writing – review & editing, Funding acquisition, Writing – original draft, Conceptualization, Supervision. **Guijie Sang:** Writing – original draft, Conceptualization, Methodology, Writing – review & editing, Formal analysis.

Data availability

All data underpinning this publication are openly available from the University of Liverpool's Research Data Catalogue at doi: 10.17638/datacat.liverpool.ac.uk/3028.

Declaration of Competing Interest

The authors declare that they have no known competing financial interests or personal relationships that could have appeared to influence the work reported in this paper.

Acknowledgements

This research was funded by the BAM Nuttall/Royal Academy of Engineering Research Chair in *Biomineral Technologies for Ground Engineering*. The contribution of El Mountassir was supported by a UKRI Future Leaders Fellowship (MR/V025376/1).

Appendix A. Supporting information

Supplementary data associated with this article can be found in the online version at doi:10.1016/j.bgtech.2025.100189.

References

Al Qabany, A., & Soga, K. (2013). Effect of chemical treatment used in MICP on engineering properties of cemented soils. *Géotechnique, 63*, 331–339. https://doi.org/10.1680/geot.SIP13.P.022

Cheng, L., Cord-Ruwisch, R., & Shahin, M. A. (2013). Cementation of sand soil by microbially induced calcite precipitation at various degrees of saturation. *Canadian Geotechnical Journal, 50*, 81–90. https://doi.org/10.1139/cgj-2012-0023

Cheng, L., Shahin, M. A., Asce, M., Mujah, D., & Scholar, P. (2017). Influence of key environmental conditions on microbially induced cementation for soil stabilization. *Journal of Geotechnical and Geoenvironmental Engineering, 143*. https://doi.org/10.1061/(ASCE)GT.1943-5606.0001586

Cheng, L., Shahin, M. A., & Cord-Ruwisch, R. (2014). Bio-cementation of sandy soil using microbially induced carbonate precipitation for marine environments. *Geotechnique, 64*, 1010–1013. https://doi.org/10.1680/geot.14.T.025

Choi, S.-G., Wu, S., & Chu, J. (2016). Biocementation for sand using an eggshell as calcium source. *Journal of Geotechnical and Geoenvironmental Engineering, 142*, Article 06016010. https://doi.org/10.1061/(ASCE)GT.1943-5606.0001534

Cui, M. J., Zheng, J. J., Zhang, R. J., Lai, H. J., & Zhang, J. (2017). Influence of cementation level on the strength behaviour of bio-cemented sand. *Acta Geotechnica, 12*, 971–986. https://doi.org/10.1007/s11440-017-0574-9

El Mountassir, G., Minto, J. M., van Paassen, L. A., Salifu, E., & Lunn, R. J. (2018). Applications of microbial processes in geotechnical engineering. *Advances in Applied Microbiology, 104*, 39–91. https://doi.org/10.1016/BS.AAMBS.2018.05.001

Gowthaman, S., Iki, T., Nakashima, K., Ebina, K., & Kawasaki, S. (2019). Feasibility study for slope soil stabilization by microbial induced carbonate precipitation (MICP) using indigenous bacteria isolated from cold subarctic region. *SN Applied Sciences, 1*, 1–16. https://doi.org/10.1007/s42452-019-1508-y

Li, D., Tian, K., Zhang, H., Wu, Y., Nie, K., & Zhang, S. (2018). Experimental investigation of solidifying desert aeolian sand using microbially induced calcite precipitation. *Construction and Building Materials, 172*, 251–262. https://doi.org/10.1016/J.CONBUILDMAT.2018.03.255

Li, M., Wen, K., Li, Y., & Zhu, L. (2017). Impact of oxygen availability on microbially induced calcite precipitation (MICP) treatment. *Geomicrobiol Journal, 35*, 15–22. https://doi.org/10.1080/01490451.2017.1303553

Liu, L., Liu, H. L., Stuedlein, A., Evans, T. M., & Xiao, Y. (2019). Strength, stiffness, and microstructure characteristics of biocemented calcareous sand. *Canadian Geotechnical Journal, 56*(10), 1502–1513. https://doi.org/10.1139/cgj-2018-0007

Ma, G., Xiao, Y., He, X., Li, J., Chu, J., & Liu, H. (2022). Kaolin-nucleation-based biotreated calcareous sand through unsaturated percolation method. *Acta Geotechnica, 17*, 3181–3193. https://doi.org/10.1007/S11440-022-01459-Y/FIGURES/12

Mahawish, A., Bouazza, A., & Gates, W. P. (2018). Improvement of coarse sand engineering properties by microbially induced calcite precipitation. *Geomicrobiol Journal, 35*, 887–897. https://doi.org/10.1080/01490451.2018.1488019;WGROUP:STRING:PUBLICATION

Mahawish, A., Bouazza, A., & Gates, W. P. (2016). Biogrouting coarse materials using soil-lift treatment strategy. *Canadian Geotechnical Journal, 53*, 2080–2085. https://doi.org/10.1139/cgj-2016-0167

Rowshanbakht, K., Khamehchiyan, M., Sajedi, R. H., & Nikudel, M. R. (2016). Effect of injected bacterial suspension volume and relative density on carbonate precipitation resulting from microbial treatment. *Ecological Engineering, 89*, 49–55. https://doi.org/10.1016/J.ECOLENG.2016.01.010

Sang, G., Lunn, R. J., El Mountassir, G., & Minto, J. M. (2023). Meter-scale MICP improvement of medium graded very gravelly sands: Lab measurement, transport modelling, mechanical and microstructural analysis. *Engineering Geology, 324*, Article 107275. https://doi.org/10.1016/j.enggeo.2023.107275

Sang, G., Lunn, R. J., El Mountassir, G., Minto, J. M., McLachlan, E., Bradley, D., & Henderson, K. (2024a). Improving non-uniform gravelly sand using microbially induced carbonate precipitation: An outdoor cubic-meter scale trial by engineering contractors. *Engineering Geology*Article 107791. https://doi.org/10.1016/J.ENGGEO.2024.107791

Sang, G., Lunn, R. J., Minto, J. M., & El Mountassir, G. (2024b). Microbially induced carbonate precipitation for soil improvement: Insights from a meter-scale radial grouting trial. *Biogeotechnics*Article 100157. https://doi.org/10.1016/J.BGTECH.2024.100157

Terzis, D., & Laloui, L. (2018). 3-D micro-architecture and mechanical response of soil cemented via microbial-induced calcite precipitation. 2018 8:1 *Scientific Reports, 8*, 1–11. https://doi.org/10.1038/s41598-018-19895-w

van Paassen, L. A., Ghose, R., Linden, T. J. M. van der, Star, W. R. L. van der, & Loosdrecht, M. C. M. van (2010). Quantifying Biomediated Ground Improvement by Ureolysis: Large-Scale Biogrout Experiment. *Journal of Geotechnical and Geoenvironmental Engineering, 136*, 1721–1728. https://doi.org/10.1061/(ASCE)GT.1943-5606.0000382

Whiffin, V. S., van Paassen, L. A., & Harkes, M. P. (2007). Microbial carbonate precipitation as a soil improvement technique. *Geomicrobiol Journal, 24*, 417–423. https://doi.org/10.1080/01490450701436505

Wu, S., Li, B., & Chu, J. (2020). Large-scale model tests of biogrouting for sand and rock. *Proceedings of the Institution of Civil Engineers-Ground Improvement*. https://doi.org/10.1680/JGRIM.18.00074

Xiao, P., Liu, H., Xiao, Y., Stuedlein, A. W., & Evans, T. M.. (2018). Liquefaction resistance of bio-cemented calcareous sand. *Soil Dynamics and Earthquake Engineering, 107*, 9–19. https://doi.org/10.1016/j.soildyn.2018.01.00

Xiao, Y., He, X., Evans, T. M., Stuedlein, A. W., & Liu, H. (2019). Unconfined compressive and splitting tensile strength of basalt fiber–reinforced biocemented sand. *Journal of Geotechnical and Geoenvironmental Engineering, 145*, Article 04019048. https://doi.org/10.1061/(ASCE)GT.1943-5606.0002108